Adsorption of Direct Yellow 12 onto Ordered Mesoporous Carbon and Activated Carbon

Fengling Liu, Jiahong Wang, Liyuan Li, Yun Shao, Zhaoyi Xu, and Shourong Zheng*

State Key Laboratory of Pollution Control and Resource Reuse, School of the Environment, Nanjing University, Nanjing 210093, People's Republic of China

Mesoporous carbon CMK-3 was prepared using a mesoporous silica SBA-15 as the template, and the adsorption of aqueous direct yellow 12 (DY-12) on CMK-3 and commercial powdered activated carbon (PAC) was studied. X-ray diffraction, N_2 adsorption, and transmission electron microscopy results demonstrate that CMK-3 with ordered structure is a true replica of its template SBA-15. CMK-3 and PAC have comparable pore volumes, whereas CMK-3 mainly consists of mesopores, and PAC contains both micropores and mesopores. The adsorption of DY-12 over CMK-3 and PAC could be well-described by the Langmuir isotherm model. The maximum adsorption amounts of CMK-3 and PAC for DY-12 at 25 °C were found to be (303.0 and 161.3) $mg \cdot g^{-1}$, respectively, indicative of a substantially higher adsorption capacity of CMK-3 compared to that of PAC. DY-12 adsorption processes over CMK-3 and PAC obey pseudosecond-order kinetics. For DY-12 adsorption on CMK-3, the rate constants were ($2.82 \cdot 10^{-4}$, $4.43 \cdot 10^{-5}$, and $9.77 \cdot 10^{-6}$) $g \cdot mg^{-1} \cdot s^{-1}$ at initial DY-12 concentrations of (17.7, 44.3, and 145) $mg \cdot dm^{-3}$, respectively. In the case of PAC, the rate constants were found to be ($1.78 \cdot 10^{-5}$, $9.8 \cdot 10^{-7}$, and $6.7 \cdot 10^{-7}$) $g \cdot mg^{-1} \cdot s^{-1}$ at initial concentrations of (17.7, 44.6, and 339) $mg \cdot dm^{-3}$, respectively, reflecting much lower adsorption rates over PAC than those over CMK-3. Furthermore, the intraparticle diffusion of DY-12 over CMK-3 and PAC was elucidated using the Weber−Morris model. The present results clearly verify the importance of mesopores in the adsorption of aqueous DY-12.

Introduction

Synthetic dye is one of the representative organic pollutants originating from chemical and textile industries. Ground and surface water contaminated by synthetic dyes may induce mutagenic activity.[1,2] Dye contamination also poses negative effects on aquatic life via obstructing light penetration and oxygen transfer into water bodies. It has been well-recognized that most synthetic dyes are highly recalcitrant to biodegradation because of their xenobiotic nature.[3] Therefore, it is desirable to develop effective treatment techniques for the removal of synthetic dyes in water prior to their discharge into the natural environment.

Advanced oxidation processes (AOPs), such as ozone oxidation, sono-oxidation, or photocatalysis, are believed to be effective for the decomposition of synthetic dyes, while AOPs generally require high treatment cost.[4,5] Adsorption treatment provides a simple and universal approach to effectively remove organic pollutants in water. Activated carbon is the most practical adsorbent used in the adsorption and separation processes because of its prominent adsorption affinity and adsorption capacity toward a variety of organic contaminants in aqueous solution. It should be emphasized that most synthetic dyes are bulky molecules in nature. Activated carbon, however, predominantly consists of micropores and normally shows low adsorption capacities for bulky pollutants because of the size exclusion effect,[6,7] by which the bulky pollutants are prevented from sufficiently accessing the micropores of the adsorbent. Recently, much research attention has been paid to synthesize carbonaceous adsorbents with amended pore structures suitable for effective adsorption of bulky molecules. For example, Tamai et al.[8] prepared activated carbons with an extremely high mesopore ratio and systematically studied their adsorption properties for a variety of giant molecules. Nakagawa et al.[9] synthesized highly mesoporous activated carbons from solid wastes for the adsorption of a reactive dye black 5 and phenol and attributed the relatively large adsorption capacity for black 5 to the plentiful mesopores in the synthesized activated carbon. Similarly, Tamai et al.[10] compared the adsorption of acid dyes with varied molecular dimensions onto a mesoporous activated carbon fiber and concluded that the mesopores played a crucial role in the adsorption of dyes with large molecular sizes.

It should be pointed out that the synthesized carbonaceous adsorbents commonly consist of both micropores and mesopores with a broad pore size distribution, and it is still challenging to clearly understand the precise mechanism controlling the adsorption of bulky pollutants to the adsorbents. Since Ryoo et al.[11] first synthesized a highly ordered mesoporous carbon, CMK-1, with MCM-48 as the template in 1999, ordered mesoporous carbons have been extensively used as adsorbents for the adsorption of bioactive giant molecules.[12−16] However, only a few studies have been conducted on the adsorption of dye molecules over ordered mesoporous carbons.[17]

In this study, ordered mesoporous carbon CMK-3 was prepared using a mesoporous silica SBA-15 as the template, and the adsorption of direct yellow 12 (DY-12) on CMK-3 was investigated. The DY-12 molecular structure as well as its molecular size estimated using Chem3D program is given in Figure 1. For comparison purposes, the adsorption of DY-12 over a commercial powdered activated carbon (PAC) was also

* Corresponding author. Tel.: +86-25-83595831. Fax: +86-25-83707304. E-mail address: srzheng@nju.edu.cn.

10.1021/je900391p CCC: $40.75
Published on Web 08/17/2009

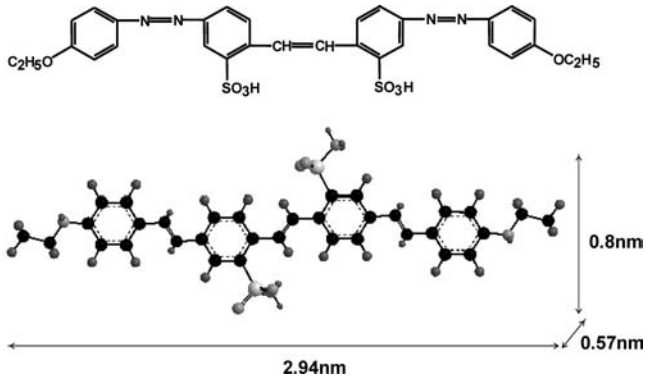

Figure 1. Molecular structure and estimated molecular size of DY-12.

carried out. The results demonstrate that CMK-3 exhibits considerable advantages over PAC in terms of adsorption capacity and adsorption kinetics.

Experimental Section

PAC. Commercial PAC obtained from Huajing Co., China, was a coconut shell-based PAC.

Material Preparation. Mesoporous silica SBA-15 was synthesized with a triblock copolymer, $EO_{20}PO_{70}EO_{20}$ (Pluronic P123, Aldrich), as the surfactant, and tetraethyl orthosilicate with a mass fraction purity of 0.98 was obtained from Shanghai Chemical Co. as the silica source.[18] Briefly, 8.0 g of P123 was dissolved in 300 cm^3 of 2 $mol \cdot kg^{-1}$ of HCl at a temperature of 40 °C under stirring, and 16.64 g of tetraethoxysilane was added. The mixture was stirred at a temperature of 40 °C for a time of 24 h, then transferred into a Teflon-lined stainless-steel autoclave, and maintained at a temperature of 80 °C for a further 48 h. The resultant precipitate was recovered by filtration, washed with distilled water, and dried at a temperature of 80 °C for a time of 10 h and then exposed to air at a temperature of 550 °C for a further 6 h to remove the organic material.

Mesoporous carbon, CMK-3, was prepared using SBA-15 as the template and sucrose as the carbon source.[19] Typically, in this procedure, 4 g of SBA-15 was mixed with 20 cm^3 of aqueous solution containing 5 g of sucrose and 0.56 g of concentrated H_2SO_4. The mixture was placed in an oven at a temperature of 100 °C for 6 h after which the temperature was increased to 160 °C for a further 6 h. The resultant material was ground and mixed with 20 cm^3 of aqueous solution containing 3.2 g of sucrose and 0.36 g of concentrated H_2SO_4, which was again subjected to the same thermal treatment as described in the previous sentence. The composite was then carbonized by flowing nitrogen over the sample at a temperature of 850 °C for a time of 5 h. The resultant black powders were treated with HF(aq) of mass fraction 0.1 at room temperature to remove the siliceous, and the CMK-3 was obtained by filtration followed by washing with distilled water and drying at a temperature of 120 °C for 4 h.

Material Characterization. Powder X-ray diffraction (XRD) patterns of SBA-15 and CMK-3 were collected in a range angles from (0.5 to 5) deg with a Rigaku D/max-RA powder diffraction meter using Cu Kα radiation. Transmission electron microscopy (TEM) images of the samples were collected on a JEM-200CX electron microscope. N_2 adsorption−desorption isotherms of the adsorbents were obtained on a Micrometrics ASAP 2020 apparatus at a temperature of −196 °C ($T = 77$ K). Prior to N_2 adsorption measurements, CMK-3 and PAC were activated at a temperature of 250 °C under vacuum for 3 h, while the dye loaded adsorbents were activated at a temperature of 100 °C under vacuum for 3 h.

Adsorption Isotherms. The adsorption of aqueous DY-12 to CMK-3 and commercial PAC were conducted using batch adsorption tests. In this approach, a series of Teflon capped glass tubes containing 0.01 g of adsorbent and 25 cm^3 of DY-12 solution with initial concentrations ranging from (15 to 400) $mg \cdot dm^{-3}$ were shaken at a temperature. To reach equilibrium, the adsorption was permitted for a time of 24 h for CMK-3 and 96 h for PAC. The adsorbent particles were removed by filtration using a 0.45 μm filter membrane and the residual DY-12 concentration measured with a UV−visible spectrometer at a wavelength of 400 nm. The equilibrium adsorption was determined from:

$$q_e = (C_0 - C_e)V/M \quad (1)$$

where q_e is the equilibrium adsorption amount, C_0 the initial DY-12 concentration, C_e the equilibrium concentration, V the volume of DY-12 solution, and M the mass of adsorbent.

To verify the pores available for DY-12, samples with known DY-12 concentrations were prepared for N_2 adsorption characterization. In this work, 500 cm^3 of DY-12 solution with known initial concentrations were added into a flask containing 200 mg of adsorbent, which was isothermally shaken at 25 °C for a time of 24 h for CMK-3 and 96 h for PAC. DY-12 loaded adsorbent was recovered by filtration followed by drying at a temperature of 50 °C for a time of 24 h and the residual DY-12 concentration in the filtrates determined spectraphotometrically. The quantity of DY-12 was estimated from eq 1. The resulting materials are referred to as CMK-3-X and PAC-X, respectively, where X denotes the quantity of DY-12.

DY-12 adsorption kinetics over CMK-3 and PAC was evaluated at three DY-12 loading levels. The initial DY-12 concentrations for adsorption kinetics over CMK-3 and PAC were calculated on the basis of corresponding adsorption isotherms to achieve approximately comparable equilibrium adsorption amounts for different adsorbents. For a typical run, 50 cm^3 of distilled water was first mixed with 200 mg of adsorbent in a 500 cm^3 flask for about 600 s. To this was added 450 cm^3 of DY-12 with a known initial concentration, and the mixture was stirred in an isothermal incubator at a temperature of 25 °C. Aliquots of a volume of about 2 cm^3 were acquired from the fluid as a function of time to spectroscopically determine the DY-12 concentration determined from:

$$q_t = (C_0 - C_t)V/M \quad (2)$$

where q_t is the adsorption at time t and C_t the DY-12 concentration at time t.

Results and Discussion

Material Characterization. Figure 2 shows the small-angle XRD patterns of SBA-15, CMK-3, and DY-12 loaded CMK-3. The XRD pattern of SBA-15 displayed three distinct diffraction peaks with 2θ at (0.96, 1.66, and 1.90) deg indexed as (100), (110), and (200) reflections of *p*6 *mm* hexagonal symmetry, clearly reflecting the ordered mesoporous structure of SBA-15.[18,20] In parallel, the XRD pattern of CMK-3 also showed the strong (100) reflection peak as well as the weak (110) and (200) reflection peaks (see CMK-3·5 in Figure 2) characteristic of the *p*6 *mm* hexagonal symmetry, suggesting that the resultant CMK-3 is an inverse replica of SBA-15.[19,21,22] The structural parameters of SBA-15 and CMK-3 were calculated, and the results are listed in Table 1. The cell parameters (a_0) of SBA-15 and CMK-3 were found to be (10.6 and 9.4) nm, respectively, suggesting a slightly higher cell dimension of SBA-15 compared to that of CMK-3. The small cell parameter of CMK-3 compared

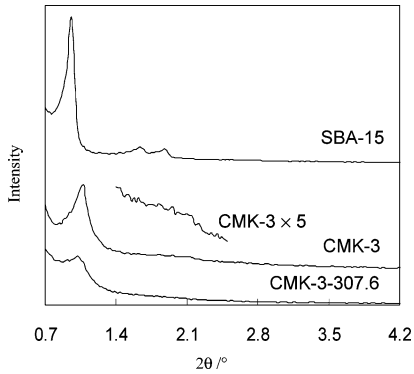

Figure 2. Small angle XRD patterns of SBA-15, CMK-3, and DY-12 loaded CMK-3.

Table 1. Structural Parameters of CMK-3 and PAC Samples

sample	a_0[a] nm	D_{mp}[b] nm	D_a[c] nm	S_{BET} $m^2 \cdot g^{-1}$	V_{micro} $cm^3 \cdot g^{-1}$	V_{meso} $cm^3 \cdot g^{-1}$	V_t[d] $cm^3 \cdot g^{-1}$
SBA-15	10.6						
CMK-3	9.4	3.75	4.3	901.2	0.02[e]	0.95[f]	0.97
CMK-3-307.6	9.4	4.16	3.4	559.6	0.0[e]	0.48[f]	0.48
PAC			3.3	1090.7	0.45[g]	0.46[h]	0.91
PAC-161.3			2.4	605.9	0.23[g]	0.13[h]	0.36

[a] Unit cell, calculated from $a_0 = 2d_{100}/(3)^{1/2}$. [b] Most probable pore diameter, calculated using the BJH method. [c] Average pore diameter, calculated from 4 V_t/S_{BET}. [d] Total pore volume, at $P/P_0 = 0.97$. [e] Micropore volume, calculated by $V_t - V_{meso}$. [f] Mesopore volume, calculated using the BJH method. [g] Micropore volume, calculated using the H−K method. [h] Mesopore volume, calculated by $V_t - V_{micro}$.

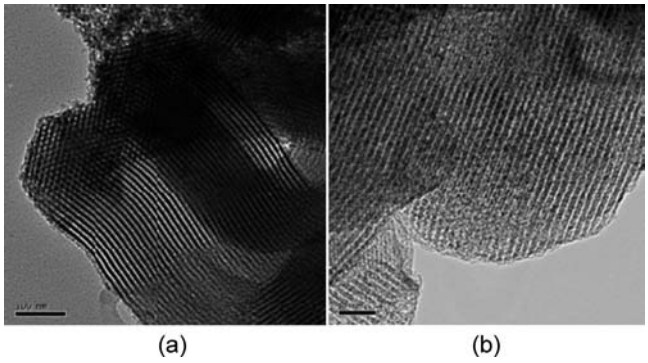

Figure 3. TEM of (a) SBA-15 and (b) CMK-3.

with its template SBA-15 mainly results from the structural shrinkage of the silica template during the replication of SBA-15.[23,24] For the DY-12 loaded CMK-3 sample, the (100) reflection as well as (110) and (200) reflections were still visible, while the reflection peak intensities substantially decreased upon DY-12 adsorption. Hartmann et al.[25] studied vitamin E adsorption on mesoporous carbons and attributed the decreased reflection peak intensity to an increased contrast in density between the carbon wall and the adsorbed vitamin E. Similarly, Liu et al.[26] studied the adsorption of nonylphenol ethoxylates over CMK-3 and ascribed the decreased reflection peak intensity to the filling of nonylphenol ethoxylates in the pores instead of the decreased structural order of the adsorbent. DY-12 loaded CMK-3 can be regenerated by washing using ethanol, and the regenerated CMK-3 has a similar XRD pattern to that of fresh CMK-3 (data not shown) that is indicative of the structural stability of CMK-3 during DY-12 adsorption. TEM images of SAB-15 and CMK-3 samples are compared in Figure 3. As shown in Figure 3, the ordered structures of SBA-15 and CMK-3 samples with hexagonal symmetry and uniform pore

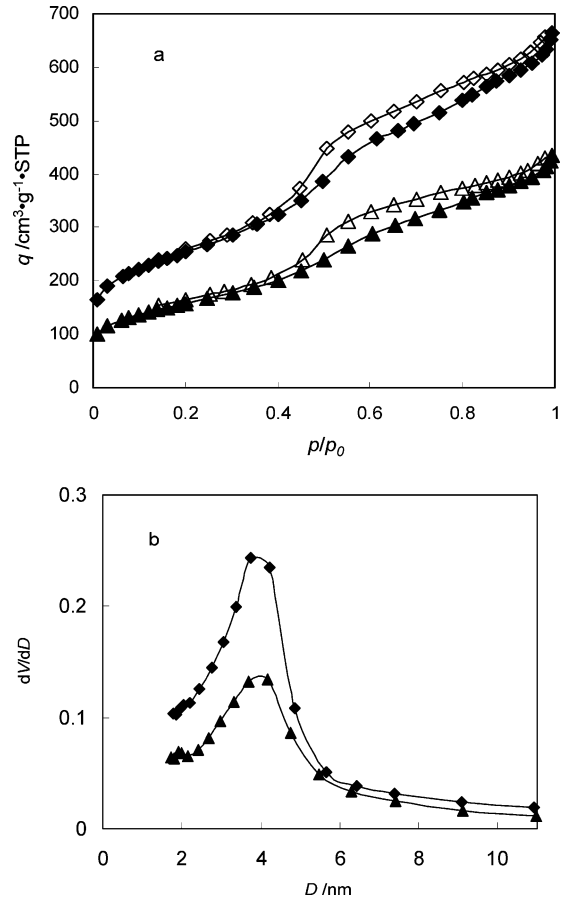

Figure 4. (a) N_2 adsorption−desorption isotherms: ◆ and ◇, CMK-3; ▲ and △, CMK-3-307.6. (b) Pore size distributions: ◆, CMK-3; ▲, CMK-3-307.6. Filled symbols denote adsorption data, and open symbols denote desorption data.

dimension were clearly observed, also suggesting that CMK-3 is a true replica of SBA-15.

N_2 adsorption isotherms of CMK-3 and PAC are shown in Figures 4 and 5, respectively. For CMK-3, the mesopore volume (V_{meso}) and pore size distribution were calculated using the Barrett−Joyner−Halenda (BJH) method.[27] The micropore volume (V_{micro}) and pore size distribution of PAC were evaluated using the Horvath−Kawazoe (H−K) model.[28] As shown in Figure 4a, CMK-3 and CMK-3-307.6 exhibited the type IV isotherm bearing an H1 hysteresis loop with the capillary condensation in the adsorption branch at pressures relative to p_0 between 0.40 and 0.66, indicative of the presence of mesopores. In comparison with CMK-3, the capillary condensation in the N_2 adsorption isotherm of CMK-3-307.6 was considerably attenuated, implying the decreased mesopore volume after DY-12 adsorption. Similar trends were also observed from the pore size distributions of CMK-3 and CMK-3-307.6. For CMK-3, a narrow pore size distribution was observed, and the most probable pore diameter (D_{mp}) calculated using the BJH method was found to be 3.75 nm. In the case of CMK-307.6, D_{mp} was determined to be 4.16 nm, approximately identical to that of CMK-3, while DY-12 adsorption leads to substantial decreases in the differential pore volumes, suggesting that DY-12 are adsorbed in the mesopores of CMK-3 and the mesopores of CMK-3 are fully accessible for DY-12 molecules. The results are further supported by the structural parameters of CMK-3 and CMK-3-307.6. As shown in Table 1, the micropore and mesopore volumes of CMK-3 are (0.02 and 0.95) $cm^3 \cdot g^{-1}$, respectively, suggesting that CMK-3 predominantly

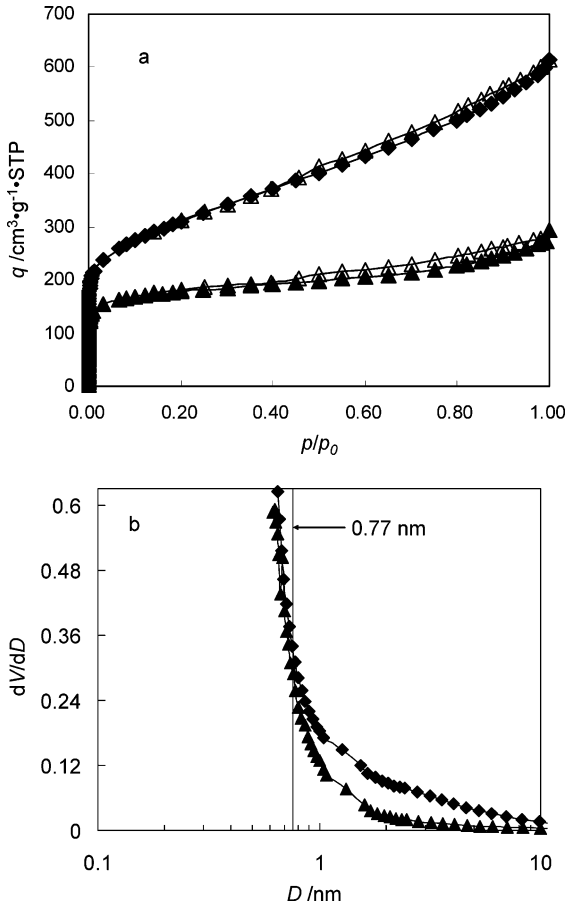

Figure 5. (a) N_2 adsorption−desorption isotherms: ◆ and ◇, PAC; ▲ and △, PAC-161.3. (b) Pore size distributions: ◆, PAC; ▲, PAC-161.3. Filled symbols denote adsorption data, and open symbols denote desorption data.

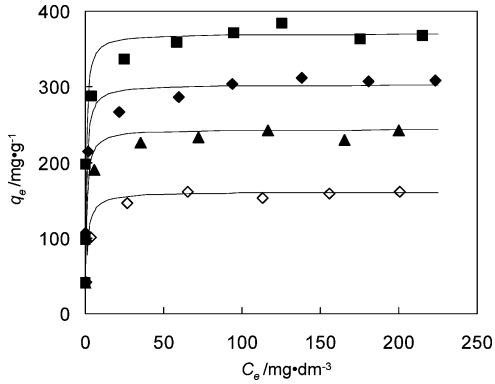

Figure 6. DY-12 adsorption isotherms over CMK-3 at: ■, $T = 318.15$ K; ◆, $T = 298.15$ K; ▲, $T = 288.15$K; and over PAC at: ◇, $T = 298.15$ K. Solid lines represent the fitting curves using the Langmuir adsorption model.

Table 2. Parameters of DY-12 Adsorption Isotherms over CMK-3 and PAC Using the Langmuir Model

sample	T / K	q_∞ / mg·g^{-1}	b / dm^3·mg^{-1}	R^2
CMK-3	288.15	243.9	1.41	0.99
CMK-3	298.15	303.0	1.57	0.98
CMK-3	318.15	370.4	1.93	0.99
PAC	298.15	161.3	0.45	0.99

consists of mesopores. The adsorption of 307.6 mg·g^{-1} of DY-12 leads to the decrease of mesopore volume from (0.95 to 0.48) cm^3·g^{-1}, clearly indicating the occupation of CMK-3 mesopores by DY-12.

Table 3. Thermodynamic Parameters for DY-12 Adsorption onto CMK-3

T / K	ΔG / kJ·mol^{-1}	ΔH / kJ·mol^{-1}	ΔS / J·K^{-1}·mol^{-1}	R^2
288.15	−32.8			
298.15	−34.2	8.0	141.6	0.99
318.15	−37.1			

N_2 adsorption isotherms of PAC and DY-12 loaded PAC are shown in Figure 5. For PAC, as the relative pressure increased, N_2 adsorption amount in PAC increased steeply when the pressure was below $0.01 \cdot p_0$ and then increased smoothly afterward, suggesting that mesopores are present in PAC. In contrast to PAC, DY-12 loaded PAC exhibited a much milder augment of N_2 adsorption amount at both low and high p/p_0, probably due to the occupation of both micropores and mesopores by DY-12. This speculation can be further verified by the pore size distributions of PAC and PAC-161.3 as shown in Figure 5b. For PAC, a broad pore size distribution was observed. In comparison with PAC, DY-12 adsorption leads to marked decreases of differential pore volumes with a pore diameter above 0.77 nm, whereas the differential pore volumes with a pore diameter below 0.77 nm are similar to those of PAC, suggesting that the pores larger than 0.77 nm are accessible for DY-12 molecules. Furthermore, the micropore and mesopore volumes of PAC are (0.45 and 0.46) cm^3·g^{-1}, respectively, suggesting that PAC consists of both micropores and mesopores (see Table 1). Upon DY-12 adsorption, the

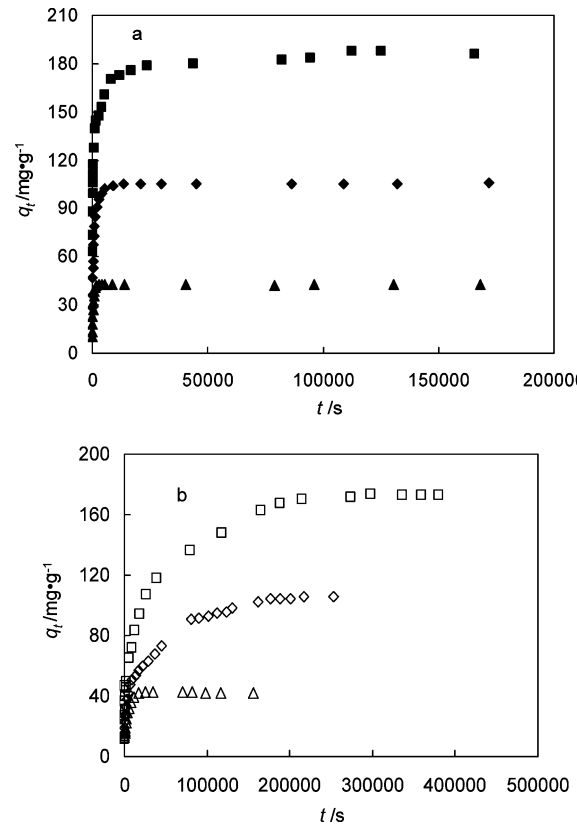

Figure 7. Time-resolved DY-12 adsorption at $T = 298.15$ K onto (a) CMK-3 with initial concentrations of ▲, $C_0 = 17.7$ mg·g^{-1}; ◆, $C_0 = 44.3$ mg·g^{-1}; ■, $C_0 = 145$ mg·g^{-1}; and (b) PAC with initial concentrations of ◇, $C_0 = 17.7$ mg·g^{-1}; △, $C_0 = 44.6$ mg·g^{-1}; □, $C_0 = 339$ mg·g^{-1}.

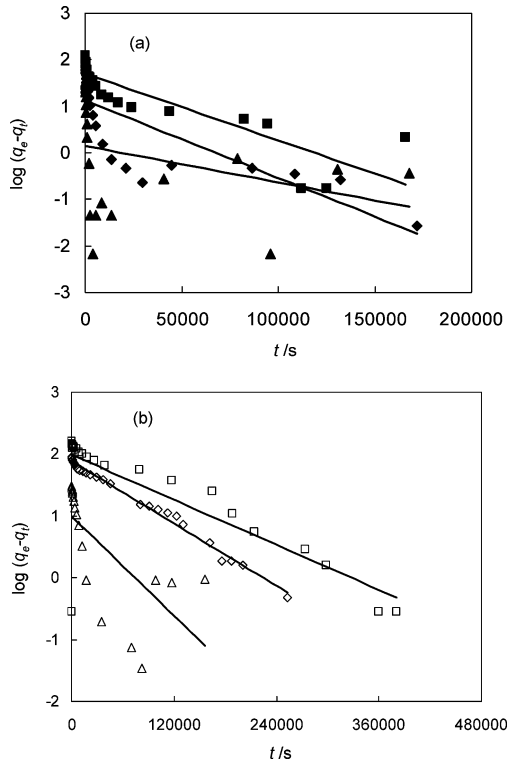

Figure 8. Simulation of DY-12 adsorption using pseudofirst-order kinetics over (a) CMK-3 with initial concentrations of ▲, $C_0 = 17.7$ mg·g^{-1}; ◆, $C_0 = 44.3$ mg·g^{-1}; ■, $C_0 = 145$ mg·g^{-1}; and (b) PAC with initial concentrations of △, $C_0 = 17.7$ mg·g^{-1}; ◇, $C_0 = 44.6$ mg·g^{-1}; □, $C_0 = 339$ mg·g^{-1}.

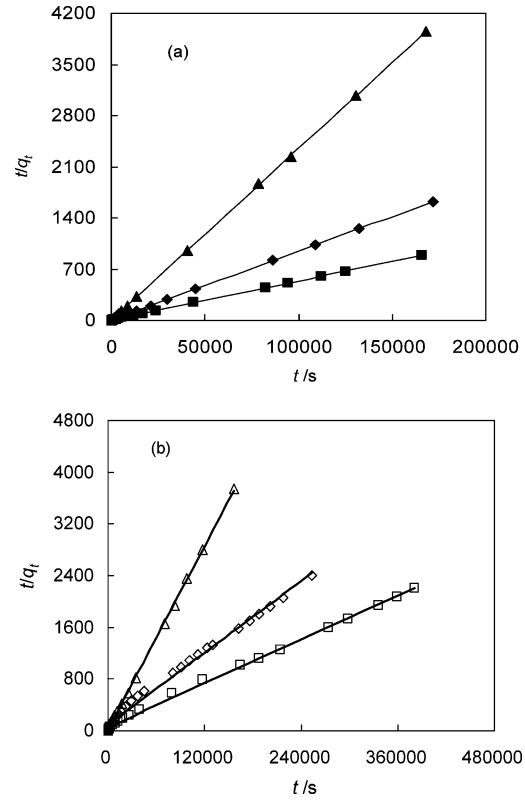

Figure 9. Simulation of DY-12 adsorption using pseudosecond-order kinetics over (a) CMK-3 with initial concentrations of ▲, $C_0 = 17.7$ mg·g^{-1}; ◆, $C_0 = 44.3$ mg·g^{-1}; ■, $C_0 = 145$ mg·g^{-1}; and (b) PAC with initial concentrations of △, $C_0 = 17.7$ mg·g^{-1}; ▲, $C_0 = 44.6$ mg·g^{-1}; □, $C_0 = 339$ mg·g^{-1}.

micropore and mesopore volumes are (0.23 and 0.13) cm^3·g^{-1}, indicating that both micropores and mesopores are occupied by DY-12 molecules.

Adsorption Isotherms. The adsorption isotherms of DY-12 over CMK-3 and PAC are compared in Figure 6. DY-12 adsorption over both CMK-3 and PAC displays typical L-type adsorption isotherms. At a temperature of 25 °C, the maximum adsorption amounts of DY-12 were found to be approximately (300 and 160) mg·g^{-1} for CMK-3 and PAC, respectively, indicative of a substantially higher adsorption capacity of CMK-3 compared to that of PAC for DY-12. It is noteworthy that the pore volumes of CMK-3 and PAC are found to be (0.97 and 0.91) cm^3·g^{-1}, while CMK-3 mainly consists of mesopores and PAC consists of both micropores and mesopores. Therefore, the much higher DY-12 adsorption amount of CMK-3 than that of PAC suggests the preferential adsorption of DY-12 in the mesopores.

To clearly verify the DY-12 adsorption mechanism, the adsorption isotherms were fitted using Langmuir and Freundlich adsorption models. Simulation results showed that DY-12 adsorption on CMK-3 and PAC could be well-described using Langmuir adsorption isotherm:[29]

$$q_e = q_\infty b C_e/(1 + bC_e) \quad (3)$$

where q_∞ is the maximum adsorption amount and b is the Langmuir adsorption constant, respectively.

The fitting parameters of DY-12 adsorption on PAC and CMK-3 are listed in Table 2. At a temperature of 25 °C, DY-12 maximum adsorption amounts were 303.0 mg·g^{-1} for CMK-3 and 161.3 mg·g^{-1} for PAC, suggesting a higher adsorption capacity of CMK-3 than that of PAC. N_2 adsorption results show that CMK-3 mainly consists of mesopores with the most probable pore diameter of 3.75 nm, which are fully accessible for DY-12. Therefore, the maximum adsorption amount is only dependent on adsorption thermodynamics. However, PAC consists of both micropores and mesopores with a broad pore size distribution. Considering that the molecular size of DY-12 is $0.57 \times 0.8 \times 2.94$ nm^3, it is rationally expected that DY-12 adsorption in the micropores with pore diameters below 0.8 nm is sterically prohibited owing to size exclusion, as evident from the pore size distribution of PAC-161.3 with pore diameters below 0.77 nm, which are similar to that of PAC. Therefore, the markedly higher maximum adsorption amount of CMK-3 for DY-12 can be attributed to its higher accessible pore volume than that of PAC, although both adsorbents contain almost identical total pore volumes.

It is interesting to note that Langmuir adsorption constants b are 1.57 and 0.45 for DY-12 adsorption over CMK-3 and PAC (see Table 2), respectively. In principle, the Langmuir adsorption constant is characteristic of the affinity of DY-12 to the adsorbent. The substantially larger Langmuir adsorption constant reflects a stronger adsorption of DY-12 on CMK-3 compared to that on PAC. Long et al.[30] studied the adsorption of reactive dyes on polymeric adsorbents and concluded that the optimum ratio of the pore diameter to sorbate molecular diameter is about 2 to 6 for effective adsorption. For CMK-3, the most probable pore diameter is 3.75 nm, which is about five times larger than the width of the DY-12 molecule. In addition, CMK-3 pore structure is constructed via an ordered array of long carbon rods to form mesoporous channels with *p*6 *mm* hexagonal symmetry, which is especially suitable for hosting sorbate molecules with a large aspect ratio. In contrast, PAC pores are characteristic of a broad pore size distribution. N_2 adsorption analysis further

Table 4. Fitting Parameters of DY-12 Adsorption onto CMK-3 and PAC Using Pseudofirst-Order and Pseudosecond-Order Kinetic Models

	pseudofirst-order kinetic model				pseudosecond-order kinetic model			
	q_e (exp.)	q_e (cal.)	k_1 ($\cdot 10^{-5}$)		q_e (exp.)	q_e (cal.)	k_2 ($\cdot 10^{-7}$)	
sample	mg·g^{-1}	mg·g^{-1}	s^{-1}	R^2	mg·g^{-1}	mg·g^{-1}	g·mg^{-1}·s^{-1}	R^2
CMK-3	42.9	1.4	1.92	0.10	42.9	42.6	2820	1.00
CMK-3	105.8	13.3	3.84	0.63	105.8	105.3	443	1.00
CMK-3	187.7	49.6	3.46	0.76	187.7	185.2	97.7	0.99
PAC	42.8	9.9	3.07	0.47	42.8	42.4	178	1.00
PAC	106.0	77.5	1.92	0.99	106.0	107.5	9.8	0.99
PAC	173.2	98.4	1.53	0.65	173.2	175.4	6.7	0.99

Table 5. Kinetic Parameters Obtained Using Weber−Morris Model

	C_0	k_{d1}	intercept I_1		k_{d2}	intercept I_2		k_{d3}	intercept I_3	
sample	mg·dm^{-3}	mg·g^{-1}·s$^{-1/2}$	mg·g^{-1}	R^2	mg·g^{-1}·s$^{-1/2}$	mg·g^{-1}	R^2	mg·g^{-1}·s$^{-1/2}$	mg·g^{-1}	R^2
CMK-3	17.7	1.30	3.6	0.99	0.28	30.4	0.96			
CMK-3	44.3	2.14	18.0	0.97	0.52	67.4	0.97			
CMK-3	145	2.50	55.0	0.98	0.56	119.4	0.99			
PAC	17.7	0.30	9.3	0.98	0.06	32.1	0.93			
PAC	44.6	0.45	11.3	0.98	0.19	32.1	0.99	0.05	80.7	0.94
PAC	339	0.59	16.4	0.98	0.22	73.4	0.99	0.02	158.7	0.85

shows that DY-12 molecules occupy the pores with pore diameter above 0.77 nm, eventually leading to a substantially lower adsorption affinity compared to CMK-3.

The thermodynamic parameters of DY-12 adsorption onto CMK-3, such as the change in Gibbs function ΔG, enthalpy ΔH, and entropy ΔS of adsorption, can also be obtained from adsorption isotherms from following equations:[31,32]

$$\Delta G = -RT \ln b \tag{4}$$

$$\ln b = \Delta S/R - \Delta H/RT \tag{5}$$

where T is the temperature and R (taken in this work to be 8.314 J·K^{-1}·mol^{-1}) is the gas constant, respectively. The values of ΔH and ΔS were calculated from the slope and intercept from eq 5. The resultant parameters are listed in Table 3. The negative values of ΔG indicate that DY-12 adsorption on CMK-3 is spontaneous and thermodynamically favorable at all temperatures tested.[33] The positive value of ΔH reveals that DY-12 adsorption over CMK-3 is endothermic, similar to most activated carbon involved adsorption processes.[34,35] In addition, the small ΔH value suggests that DY-12 adsorption on CMK-3 is a physical adsorption process. The positive value of ΔS is characteristic of the replacement of solvent molecules on CMK-3 surface by sorbate molecules.[36,37]

Adsorption Kinetics. The time-resolved adsorption profiles of DY-12 over CMK-3 and PAC with varied initial concentrations are compared in Figure 7. For CMK-3, DY-12 adsorption reached the equilibrium after approximately (2682, 9060, and 43 890) s with the initial concentrations of (17.7, 44.3, and 145.0) mg·dm^{-3}, respectively, reflecting a higher initial concentration (adsorption amount) and longer adsorption time required to reach the adsorption equilibrium. In the case of PAC, it required (25.014, 176.44, and 298.45) ks to reach the adsorption equilibrium for DY-12 with the initial concentrations of (17.7, 44.6, and 339.0) mg·dm^{-3}. It should be pointed out that in comparison with CMK-3 the adsorption of DY-12 over PAC is substantially slow. DY-12 adsorption to PAC occurs in both mesopores and micropores. In contrast, DY-12 molecules are mainly adsorbed in the mesopores of CMK-3. Therefore, the considerably low adsorption rate can be tentatively attributed to the considerably large diffusion resistance in the micropores.

To further elucidate DY-12 adsorption kinetics over CMK-3 and PAC, pseudofirst-order and pseudosecond-order kinetic models were applied to follow the mass transfer during the DY-12 adsorption process. For pseudofirst-order kinetics, the adsorption process can be described using Lagergren's rate equation:[38]

$$\log(q_e - q_t) = \log(q_e) - k_1 t/2.303 \tag{6}$$

where k_1 is the pseudofirst-order rate constant.

The pseudosecond-order kinetics based on adsorption capacity can be expressed as follows:[39]

$$t/q_t = 1/(k_2 q_e^2) + t/q_e \tag{7}$$

where k_2 is the pseudosecond-order rate constant.

The plots of $\log(q_e - q_t)$ versus time t based on pseudofirst-order kinetics and t/q_t versus t based on the pseudosecond-order kinetics are compared in Figures 8 and 9, and the fitting parameters are listed in Table 4. The plot of $\log(q_e - q_t)$ versus t (see Figure 8) are not linear. However, linear plots of DY-12 adsorption with R^2 values higher than 0.99 were obtained for the fitting using pseudosecond-order kinetic model, suggesting that DY-12 adsorption can be well-described by pseudosecond-order kinetics. In addition, DY-12 adsorption amounts from experimental data are close to those from fitting results, further confirming that the adsorption of aqueous DY-12 onto CMK-3 and PAC obeys the pseudosecond-order kinetic model. As shown in Table 4, the rate constants of DY-12 adsorption over CMK-3 were found to be ($2.82 \cdot 10^{-4}$, $4.43 \cdot 10^{-5}$, and $9.77 \cdot 10^{-6}$) g·mg^{-1}·s^{-1} at initial DY-12 concentrations of (17.7, 44.3, and 145) mg·dm^{-3}, respectively, indicative of a much slower adsorption process at higher DY-12 adsorption amount. This is probably because at low initial DY-12 concentrations (low DY-12 adsorption amounts) DY-12 molecules quickly reach the adsorption sites located in the pore mouth region or the sites adjoining the pore mouth. At high initial concentrations (high adsorption amounts), DY-12 adsorption results in the full occupation of the adsorption sites in the pore mouth region or the sites adjoining the pore mouth, and DY-12 is adsorbed in the sites deep in the pores by penetrating through a relatively long diffusion path, eventually giving rise to a low adsorption rate. A similar trend was also observed for DY-12 adsorption over PAC.

To further verify the controlling mechanism involved in the adsorption process, the intraparticle diffusion is evaluated using Weber−Morris model:[40−42]

$$q_t = k_d t^{1/2} + I \quad (8)$$

where k_d is the intraparticle diffusion constant and I the intercept reflecting the diffusion boundary layer thickness.

The plots of q_t versus $t^{1/2}$ with varied initial concentrations are compared in Figure 10. In general, the $q_t-t^{1/2}$ relations are of multilinearity in nature, suggesting multiple adsorption steps involved in the adsorption processes.[43,44] The plots were fitted using the linear regression method, and the resultant parameters are listed in Table 5. According to Weber−Morris model, the adsorption process is controlled solely by the intraparticle diffusion provided the linear plot passes through the origin. Alternatively, the external diffusion as well as the intraparticle diffusion contributes to the global adsorption process if the straight line deviates from the origin. As shown in Figure 10a, the $q_t-t^{1/2}$ plots consist of two linear portions for DY-12 adsorption to CMK-3 with varied initial concentrations, and the extrapolation of the first linear portions does not pass through the origin, suggesting the involvement of external mass transfer. The first linear portion can be attributed to DY-12 diffusion in the mesopores of CMK-3, and the second portion is characteristic of the final equilibrium step in which intraparticle diffusion gradually slows down because of the much lower concentration difference as well as diffusion driving force. As shown in Table 5, DY-12 adsorption with a higher initial concentration results in a larger intercept of the first linear portion, attributed to the larger external mass transfer resistance during diffusion across the liquid film surrounding the adsorbent particle.[45] In parallel, increasing the initial concentration leads to the increase of the diffusion constant (k_{d1}), mainly resulting from the increased concentration gradient as well as the increased diffusion driving force.

For DY-12 adsorption to PAC, the $q_t-t^{1/2}$ plots also consist of a multilinearity, and the first linear portions deviate from the origin, reflecting the presence of external diffusion resistance.

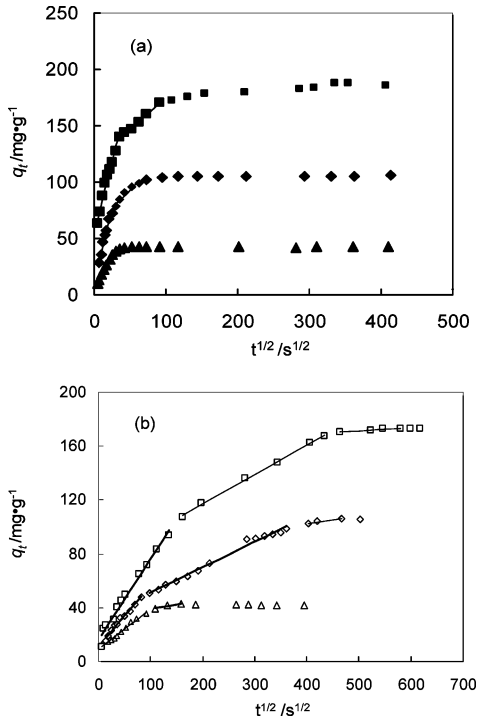

Figure 10. Intraparticle diffusion plots for DY-12 adsorption onto (a) CMK-3 with initial concentrations of ▲, C_0 = 17.7 mg·g^{-1}; ◆, C_0 = 44.3 mg·g^{-1}; ■, C_0 = 145 mg·g^{-1}; and (b) PAC with initial concentrations of △, C_0 = 17.7 mg·g^{-1}; ▲, C_0 = 44.6 mg·g^{-1}; □, C_0 = 339 mg·g^{-1}.

Similarly, increasing initial DY-12 concentrations leads to the increased intercept and slope, characteristic of the increased external diffusion resistance and enhanced diffusion rate resulting from the increased concentration gradient and diffusion driving force, respectively. As for DY-12 adsorption to PAC with an initial concentration of 17.7 mg·dm^{-3}, the $q_t-t^{1/2}$ plot presents two linear portions. The first linear portion is indicative of DY-12 diffusion into the pores of PAC, and the second one is attributed to the final equilibrium step. At initial DY-12 concentrations of (44.6 and 339) mg·dm^{-3}, three linear portions are clearly observed in the $q_t-t^{1/2}$ plots. Similarly, the third portion is ascribed to the final equilibrium step. The first and second linear portions are probably associated with DY-12 diffusion into the micropores and mesopores of PAC. It is noteworthy that the k_{d1} values of CMK-3 at different initial concentrations are higher than those of PAC, indicating markedly higher diffusion rates of DY-12 over CMK-3 compared to those over PAC.

Conclusions

Ordered mesoporous carbon CMK-3 was prepared using SBA-15 as the template, and DY-12 adsorption to CMK-3 and PAC was investigated in this study. DY-12 adsorption isotherms over CMK-3 and PAC can be well-described using Langmuir adsorption model. Although CMK-3 and PAC have comparable pore volumes, the considerably higher adsorption capacity and adsorption affinity of CMK-3 for DY-12 can be attributed to the higher mesopore fraction in CMK-3 compared to PAC. Furthermore, the mesopores of CMK-3 can be occupied by DY-12, whereas for PAC the pores with a pore diameter larger than 0.77 nm are accessible for DY-12 molecules. Adsorption kinetic results show that DY-12 adsorption over CMK-3 and PAC obeys pseudosecond-order kinetics. At similar DY-12 adsorption amounts, however, substantially larger adsorption rates are observed for DY-12 adsorption to CMK-3 than those to PAC. In terms of a diffusion mechanism, DY-12 adsorption to CMK-3 and PAC is controlled by both external mass transfer and diffusion in the pores irrespective of initial DY-12 concentration.

Literature Cited

(1) Rajaguru, P.; Vidya, L.; Baskarasethupathi, B.; Kumar, P. A.; Palanivel, M.; Kalaiselvi, K. Genotoxicity Evaluation of Polluted Ground Water in Human Peripheral Blood Lymphocytes Using the Comet Assay. *Mutat. Res.* **2002**, *517*, 29–37.

(2) Umbuzeiro, G. A.; Freeman, H.; Warren, S. H.; Oliveira, D. P.; Terao, Y.; Watanabe, T.; Claxton, L. D. The Contribution of Azo Dyes to the Mutagenic Activity of the Cristais River. *Chemosphere* **2005**, *60*, 55–64.

(3) Pandey, A.; Singh, P.; Iyengar, L. Bacterial Decolorization and Degradation of Azo Dyes. *Int. Biodeterior. Biodegrad.* **2007**, *59*, 73–84.

(4) Vandevivere, P. C.; Binachi, R.; Verstrate, W. Treatment and Reuse of Wastewater from the Textile Wet Processing Industry: Review of Emerging Technologies. *J. Chem. Technol. Biotechnol.* **1998**, *72*, 289–302.

(5) Alaton, I. A.; Balcioglu, I. A.; Bahnemann, D. W. Advanced Oxidation of a Reactive Dye Bath Effluent: Comparison of O_3, H_2O_2/UV-C and TiO_2/UV-A Process. *Water Res.* **2002**, *36*, 1143–1154.

(6) Kilduff, J. E.; Karanfil, T.; Chin, Y.-P.; Weber, W. J., Jr. Adsorption of Natural Organic Polyelectrolytes by Activated Carbon: A Size Exclusion Chromatography Study. *Environ. Sci. Technol.* **1996**, *30*, 1336–1343.

(7) Kilduff, J. E.; Karanfil, T.; Weber, W. J., Jr. Competitive Interactions among Components of Humic Acids in Granular Activated Carbon Adsorption Systems: Effects of Solution Chemistry. *Environ. Sci. Technol.* **1996**, *30*, 1344–1351.

(8) Tamai, H.; Kakii, T.; Hirota, Y.; Kumamoto, T.; Yasuda, H. Synthesis of Extremely Large Mesoporous Activated Carbon and its Unique Adsorption for Giant Molecules. *Chem. Mater.* **1996**, *8*, 454–462.

(9) Nakagawa, K.; Namba, A.; Mukai, S. R.; Tamon, H.; Ariyadejwanich, P.; Tanthapanichakoon, W. Adsorption of Phenol and Reactive Dye

from Aqueous Solution on Activated Carbons Derived from Solid Wastes. *Water Res.* **2004**, *38*, 1791–1798.
(10) Tamai, H.; Yoshida, T.; Sasaki, M.; Yasuda, H. Dye Adsorption on Mesoporous Activated Carbon Fiber Obtained from Pitch Containing Yttrium Complex. *Carbon* **1999**, *37*, 983–989.
(11) Ryoo, R.; Joo, S. H.; Jun, S. Synthesis of Highly Ordered Carbon Molecular Sieves via Template-mediated Structural Transformation. *J. Phys. Chem. B* **1999**, *103*, 7743–7746.
(12) Vinu, A.; Streb, C.; Murugesan, V.; Hartmann, M. Adsorption of Cytochrome C on New Mesoporous Carbon Molecular Sieves. *J. Phys. Chem. B* **2003**, *107*, 8297–8299.
(13) Hartmann, M. Ordered Mesoporous Materials for Bioadsorption and Biocatalysis. *Chem. Mater.* **2005**, *17*, 4577–4593.
(14) Hudson, S.; Magner, E.; Cooney, J.; Hodnett, B. K. Methodology for the Immobilization of Enzymes onto Mesoporous Materials. *J. Phys. Chem. B* **2005**, *109*, 19496–19506.
(15) Vinu, A.; Hossian, K. Z.; Srinivasu, P.; Miyahara, M.; Anandan, S.; Gokulakrishnan, N.; Mori, T.; Ariga, K.; Balasubramanian, V. V. Carboxy-mesoporous Carbon and its Excellent Adsorption Capability for Proteins. *J. Mater. Chem.* **2007**, *17*, 1819–1825.
(16) Ariga, K.; Vinu, A.; Miyahara, M.; Hill, J. P.; Mori, T. One-pot Separation of Tea Components through Selective Adsorption on Pore-engineered Nanocarbon Carbon Nanocage. *J. Am. Chem. Soc.* **2007**, *129*, 11022–11023.
(17) Yuan, X.; Zhuo, S.; Xing, W.; Cui, H.; Dai, X.; Liu, X.; Yan, Z. Aqueous Dye Adsorption on Ordered Mesoporous Carbons. *J. Colloid Interface Sci.* **2007**, *310*, 83–89.
(18) Zhao, D. Y.; Feng, J. L.; Huo, Q. S.; Melosh, N.; Fredrickson, G. H.; Chmelka, B. F.; Stucky, G. D. Triblock Copolymer Syntheses of Mesoporous Silica with Periodic 50 to 300 Angstrom Pores. *Science* **1998**, *279*, 548–552.
(19) Lee, J. S.; Joo, S. H.; Ryoo, R. Synthesis of Mesoporous Silicas of Controlled Pore Wall Thickness and their Replication to Ordered Nanoporous Carbons with Various Pore Diameters. *J. Am. Chem. Soc.* **2002**, *124*, 1156–1157.
(20) Sayari, A.; Yang, Y. SBA-15 Templated Mesoporous Carbon: New Insights into the SBA-15 Pore Structure. *Chem. Mater.* **2005**, *17*, 6108–6113.
(21) Jun, S.; Joo, S. H.; Ryoo, R.; Kruk, M.; Jaroniec, M.; Liu, Z.; Ohsuna, T.; Terasaki, O. Synthesis of New, Nanoporous Carbon with Hexagonally Ordered Mesostructure. *J. Am. Chem. Soc.* **2000**, *122*, 10712–10713.
(22) Sakintuna, B.; Yurum, Y. Templated Porous Carbons: A Review Article. *Ind. Eng. Chem. Res.* **2005**, *44*, 2893–2902.
(23) Kruk, M.; Jaroniec, M.; Ryoo, R.; Joo, S. H. Characterization of Ordered Mesoporous Carbons Synthesized using MCM-48 Silicas as Templates. *J. Phys. Chem. B* **2000**, *104*, 7960–7968.
(24) Fuertes, A. B.; Nevskaia, D. M. Control of Mesoporous Structure of Carbons Synthesised Using a Mesostructured Silica as Template. *Microporous Mesoporous Mater.* **2003**, *62*, 177–190.
(25) Hartmann, M.; Vinu, A.; Chandrasekar, G. Adsorption of Vitamin E on Mesoporous Carbon Molecular Sieves. *Chem. Mater.* **2005**, *17*, 829–833.
(26) Liu, G. M.; Zheng, S. R.; Yin, D. Q.; Xu, Z. Y.; Fan, J.; Jiang, F. Adsorption of Aqueous Alkylphenol Ethoxylate Surfactants by Mesoporous Carbon CMK-3. *J. Colloid Interface Sci.* **2006**, *302*, 47–53.
(27) Barrett, E. P.; Joyner, L. G.; Halenda, P. P. The Determination of Pore Volume and Area Distributions in Porous Substances. I. Computations from Nitrogen Isotherms. *J. Am. Chem. Soc.* **1951**, *73*, 373–380.
(28) Horvath, G.; Kawazoe, K. Method for the Calculation of Effective Pore Size Distribution in Molecular Sieve Carbon. *J. Chem. Eng. Jpn.* **1983**, *16*, 470–475.
(29) Chatzopoulos, D.; Varma, A.; Irvine, R. L. Activated Carbon Adsorption and Desorption of Toluene in the Aqueous Phase. *AIChE J.* **1993**, *39*, 2027–2041.
(30) Long, C.; Lu, Z. Y.; Li, A. M.; Liu, W.; Jiang, Z. M.; Chen, J. L.; Zhang, Q. X. Adsorption of Reactive Dyes onto Polymeric Adsorbents: Effect of Pore Structure and Surface Chemistry Group of Adsorbent on Adsorptive Properties. *Sep. Purif. Technol.* **2005**, *44*, 91–96.
(31) Murray, J. M.; Dillard, J. R. The Oxidation of Cobalt (II) Adsorbed on Manganese Dioxide. *Geochim. Cosmochim. Acta* **1979**, *43*, 781–787.
(32) Karadag, D.; Turan, M.; Akgul, E.; Tok, S.; Faki, A. Adsorption Equilibrium and Kinetics of Reactive Black 5 and Reactive Red 239 in Aqueous Solution onto Surfactant-modified Zeolite. *J. Chem. Eng. Data* **2007**, *52*, 1615–1620.
(33) Ozcan, A.; Oncu, E. M.; Ozcan, A. S. Adsorption of Acid Blue 193 from Aqueous Solutions onto DEDMA-sepiolite. *J. Hazard. Mater.* **2006**, *129*, 1–3.
(34) Namasivayam, C.; Kavitha, D. Removal of Congo Red from Water by Adsorption onto Activated Carbon Prepared from Coir Pith, an Agricultural Solid Waste. *Dyes Pigm.* **2002**, *54*, 47–58.
(35) Al-Degs, Y. S.; El-Barghouthi, M. I.; El-Sheikh, A. H.; Walker, G. M. Effect of Solution pH, Ionic Strength, and Temperature on Adsorption Behavior of Reactive Dyes on Activated Carbon. *Dyes Pigm.* **2008**, *77*, 16–23.
(36) Dizge, N.; Aydiner, C.; Demirbas, E.; Kobya, M.; Kara, S. Adsorption of Reactive Dyes from Aqueous Solutions by Fly Ash: Kinetic and Equilibrium Studies. *J. Hazard. Mater.* **2008**, *150*, 737–746.
(37) Namasivayam, C.; Yamuna, R. T. Adsorption of Chromium (VI) by a Low-cost Adsorbent: Biogas Residual Slurry. *Chemosphere* **1995**, *30*, 561–578.
(38) Trivedi, H. C.; Patel, V. M.; Patel, R. D. Adsorption of Cellulose Triacetate on Calcium Silicate. *Eur. Polym. J.* **1973**, *9*, 525–531.
(39) Mckay, G.; Ho, Y. S. Pseudo-second Order Model for Sorption Processes. *Process Biochem. (Oxford, U.K.)* **1999**, *34*, 451–465.
(40) Weber, W. J.; Morris, J. C. In *Advances in Water Pollution Research: Removal of Biologically Resistant Pollutants from Waste Waters by Adsorption*. Proceedings of International Conference on Water Pollution Symposium, 1962; Pergamon Press: Oxford; Vol. 2, pp 231−266.
(41) Guibal, E.; Saucedo, I.; Jansson-Charrier, M.; Delanghe, B.; Le Cloirec, P. Uranium and Vanadium Sorption by Chitosan and Derivatives. *Water Sci. Technol.* **1994**, *30*, 183–190.
(42) Daifullah, A. E.; El-Reefy, S.; Gad, H. Adsorption of p-Nitrophenol on Inshas Incinerator Ash and on Pyrolysis Residue of Animal Bones. *Adsorpt. Sci. Technol.* **1997**, *15*, 485–496.
(43) McKay, G. The Adsorption of Dyestuffs from Aqueous Solutions Using Activated Carbon. III. Intraparticle Diffusion Processes. *J. Chem. Technol. Biotechnol.* **1983**, *33*, 196–204.
(44) McKay, G.; Otterburn, M. S.; Sweeney, A. G. The Removal of Color from Effluent Using Various Adsorbents III. Silica: Rate processes. *Water Res.* **1980**, *14*, 15–20.
(45) Mall, I. D.; Srivastava, V. C.; Agarwal, N. K.; Mishra, I. M. Removal of Congo Red from Aqueous Solution by Bagasse Fly Ash and Activated Carbon: Kinetic study and Equilibrium Isotherm Analyses. *Chemosphere* **2005**, *61*, 492–501.

Received for review January 29, 2009. Accepted August 4, 2009. This work was supported by the National Natural Science Foundation of China (nos. 20677026, 20637030, and 20877039) and Scientific and Technical Supporting Programs of China (2006BAC02A15).

JE900391P